Catalysis Science & Technology

Accepted Manuscript

ROYAL SOCIETY OF CHEMISTRY

www.rsc.org/catalysis

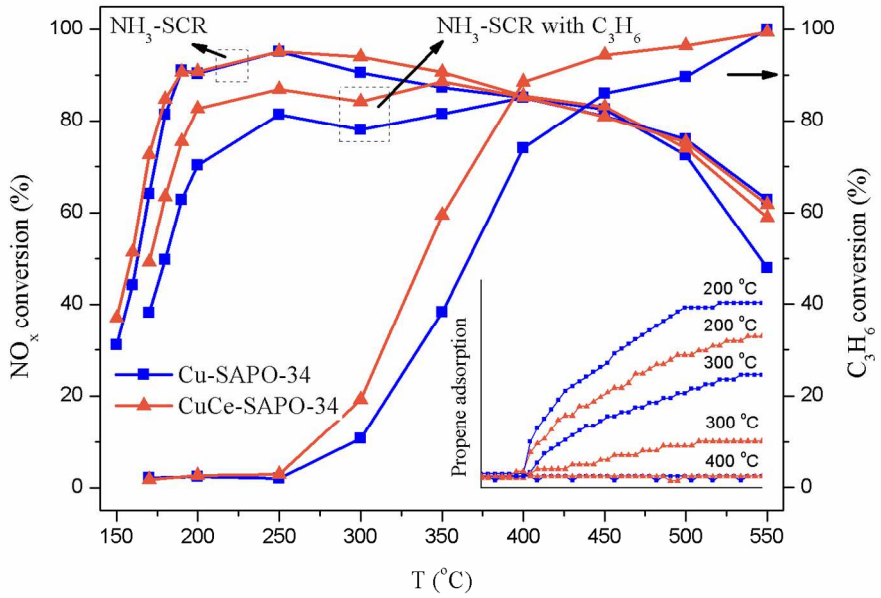

287x201mm (150 x 150 DPI)

Cerium promotion on the hydrocarbons resistance of Cu-SAPO-34 NH_3-SCR monolith catalyst

Yi Cao[1], Li Lan[1], Xi Feng[2], Zhengzheng Yang[3], Sha Zou[1], Haidi Xu[1], Zheqi Li[1], Maochu Gong[1], Yaoqiang Chen[1, 2, 3, 4*]

1. Key Laboratory of Green Chemistry & Technology of the Ministry of Education, College of Chemistry, Sichuan University, Chengdu, 610064, PR China

2. College of Chemical Engineering, Sichuan University, Chengdu, 610064, PR China

3. College of Architecture and Environment, Sichuan University, Chengdu 610064, Sichuan, PR China

4. Sichuan Province Engineering Center of Environmental Catalytic Materials, Chengdu 610064, PR China

* To whom corresponding authors should be addressed:

nic7501@scu.edu.cn (Yaoqiang Chen)

Tel. /Fax: +86 28 85418451

Abstract:

CuCe-SAPO-34 (CuCe-x) catalysts with 3 wt% Cu and various contents of Ce for selective catalytic reduction of NO_x by NH_3 (NH_3-SCR) were prepared by wet co-impregnation method. The activities of CuCe-x catalysts were better than that of Cu-SAPO-34 (Cu). In addition, hydrocarbons (HCs) resistance of the CuCe-x catalysts was examined and compared to that of Cu catalyst. The NH_3-SCR performance after

C_3H_6 poisoning of CuCe-x catalysts was preferable to that of Cu catalyst, since the C_3H_6 oxidation performance was improved by the addition of Ce. The XRD, UV-vis-DRS and H_2-TPR results confirmed that the addition of Ce could inhibit the aggregation of CuO crystallites and increase the amount of isolated copper ions. Furthermore, the NH_3-TPD and TGA results demonstrated that the addition of Ce decreased the amount and strength of strong acid sites, so that the amounts of C_3H_6/O_2 adsorption on CuCe-x catalysts were lower than that on Cu catalyst. Therefore, activity and HCs resistance of Cu-SAPO-34 was improved by the addition of Ce.

Keywords: Cerium; hydrocarbons resistance; NH_3-SCR; Cu-SAPO-34

1. Introduction:

Nitrogen oxides (NO_x) emitted from the diesel engine could lead to severe environmental issues such as acid rain, photochemical smog, ozone depletion and haze event.[1-4] NH_3-SCR has been recognized as one of the most advanced technologies for eliminating the NO_x emission. [5-7] However, the application of commercial V_2O_5/WO_3-TiO_2 catalyst was restricted due to its poor hydrothermal stability, low N_2 selectivity, narrow operating window and environmental toxicity. [8] Recently, Cu modified zeolites with small pore size (SSZ-13 and SAPO-34) NH_3-SCR catalysts have attracted much attention owing to their excellent activity, selectivity and hydrothermal stability. [9-12] However, hydrocarbons (HCs) slipped from the diesel engine, particularly during the cold start period of the engine when the temperature of the diesel oxidation catalyst (DOC) is not high enough to oxidize the HCs and/or the upstream DOC is

deactivated which cannot oxidize the HCs, and would poison the Cu-CHA catalysts. [13-15] Although HCs could be applied as the reductant in a HC-SCR process, [16-18] they are considered as poisons for NH_3-SCR catalysts. [13, 19, 20]

HCs emitted from the diesel engine contain different types, such as paraffins, olefins, and aromatics. Seo et al. [20] reported that olefins (C_3H_6) have larger negative effect on the NH_3-SCR performance of the Cu-zeolite than other HCs. In addition, Cavataio et al. [8] proposed that propylene was proven to have the most significant impact on NO_x conversion followed by n-decane and benzene for Cu-zeolite at 300 °C. Furthermore, Blakeman et al. [15] reported that the NO_x conversion of Cu-CHA catalyst did not change with the addition of n-octane, but decreased obviously with the poisoning of C_3H_6. Thus, in this study C_3H_6 was applied to determine the HCs resistance property of the Cu-SAPO-34.

The poisoning mechanism of the zeolite-based catalysts by HCs has been investigated extensively. For Cu-beta catalyst, Luo et al. [14] demonstrated that the surface acrolein-like and coke species formed by incomplete C_3H_6 oxidation inhibited the NH_3-SCR activity of the Cu-beta. In addition, over ZSM-5-based NH_3-SCR catalyst, Li et al. [21] found that the carbonaceous deposition blocked the Fe^{3+} active sites which inhibited the generation of required intermediates NO_2 and consequently decreased the NH_3-SCR performance. Heo et al. [13] reported that the competitive adsorption between C_3H_6 and NH_3 on the surface of the catalysts and the useless consumption of NH_3 by

side reaction caused the inhibition of the NH_3-SCR activity of Cu-ZSM5, and the extent of inhibition effect aggravated with the concentration of C_3H_6 increasing. Furthermore, Ye et al. [22] showed that compared with Cu-ZSM-5, zeolites with smaller pores performed better HCs resistance, and the hydrocarbon deposition which blocked the active sites could reduce the activity of the catalyst. Moreover, for the CHA-based catalyst, Ma et al. [19] found that the competitive adsorption process between NO_x and C_3H_6 as well as coke deposition on the surface of the catalyst contributed to the deactivation of Cu-CHA catalyst. Meanwhile, Lin et al. [23] and Ma et al. [24] reported that the strong acid was correlated with the coke deposition.

According to the HCs poisoning mechanism, two approaches could be proposed to improve the HCs resistance of Cu-SAPO-34: one is to create more active sites, when blocked to the same extent, the catalyst with more active sites would perform better NH_3-SCR activity, and the active sites of Cu-SAPO-34 have been proved to be isolated copper species; [25, 26] the other is to introduce a second cation into the Cu-SAPO-34 catalyst which could improve the conversion of C_3H_6 and decrease the formation of coke. Pt-containing catalysts were always applied to eliminate C_3H_6, but Pt cannot be used in Cu-SAPO-34 NH_3-SCR catalyst, as the removal of C_3H_6, NH_3 was consumed simultaneously. [27, 28] Sultana et al. [29] found that the Na doped Cu-ZSM-5 performed better HCs resistance, since the Na^+ inhibited the formation of coke. Meanwhile, CuNa-SSZ-13 was prepared by Gao et al.[30], which performed better activity than Cu-SSZ-13, but it was also proposed therein that the addition of Na would decrease the

hydrothermal stability of the zeolite. So the doped cations should promote the HCs resistance of the Cu-SAPO-34 catalyst, meanwhile, the activity and hydrothermal stability of the Cu-SAPO-34 cannot be reduced.

For oxidation catalyst, ceria was employed to improve the activity of HCs oxidation, [31, 32] and Ce could be applied as the promoter and/or active sites of NH_3-SCR catalysts, [33-36] in addition, as our previous study reported, Ce could be used to improve the activity and hydrothermal stability of Cu-SAPO-34 catalyst.[37] Herein, in this study, Ce was introduced to promote the HCs resistance of CuSAPO-34, and series CuCe-x catalysts with various contents of Ce were prepared by wet co-impregnation method. In addition, N_2 adsorption, X-ray diffraction (XRD), H_2-temperature programmed reduction (H_2-TPR), ultraviolet-visible diffuse reflectance spectrum (UV-Vis-DRS), NH_3-temperature programmed desorption (NH_3-TPD) and thermo-gravimetric analyzer (TGA) were utilized to determine the effect of Ce on the HCs resistance of Cu-SAPO-34.

2. Experimental

2.1. Catalyst preparation

A series of $CuCe_x$-SAPO-34 catalysts were prepared by a simple wet impregnation method. 1.1325 g of $Cu(NO_3)_2 \cdot 3H_2O$ (99%, Kelong) and the required amount of $Ce(NO_3)_3 \cdot 6H_2O$ (99%, Jinshan) were dissolved into 5.5 ml of deionized water, to ensure the weight fraction of Cu about 3 wt%, then the desired amount of commercial

NH_4-SAPO-34 (Nankai, Tianjin, Si/(Al + P + Si) = 0.1) was dropped into the mixed solution of $Cu(NO_3)_2$ and $Ce(NO_3)_3$ to obtain a paste, afterwards the paste was stirred at room temperature (15 °C) for 3 h followed by drying at 100 °C for 6 h and calcining at 550 °C for 3 h. Cu-SAPO-34 catalyst and a series of Ce_x-SAPO-34 catalysts were prepared by the same method above. Finally the prepared catalysts and SAPO-34 support material were coated on honeycomb cordierites (2.5 ml, 400 cpi, Jiangsu Yixing) as described in our previous study,[38] so that the monolith catalysts with a loading of ca. 130 g/L could be achieved. The chemical component of each catalyst was determined by ICP-AES method, and the results were listed in Table 1. The prepared catalysts were denoted as Cu, Ce-x and CuCe-x (x represented the weight ratio of Ce in the catalysts which could be found in the ICP-AES results).

2.2. Steady-state reactor experiments

The catalytic activity measurement was carried out in a fixed bed quartz flow reactor. Three K-type thermal-couples were placed at front face-center, back face-center and the middle of out edge of monolith catalyst, respectively, the average temperature was used to monitor the temperature of the catalyst, the temperature differences of the three thermal-couples were lower than 2 °C at the temperature below 250 °C, and no larger than 10 °C at the temperature above 250°C. Reactant gases were regulated by means of mass-flow controllers before entering the reactor. The NH_3-SCR activity test, NH_3 oxidation test,C_3H_6-SCR test, C_3H_6 oxidation test and NH_3-SCR with C_3H_6 test were performed for all catalysts and the concentrations of the simulated gases were as

follows: 350 ppm NO (when added), 350 ppm NH_3 (when added), 8 % O_2, 5 vol % H_2O, 350–1050 ppm C_3H_6 (when added) and balanced with N_2, the gas hourly space velocity (GHSV) was 30,000 h^{-1} and the total flow rate was 1250 ml/min. The concentrations of NO_x (NO and NO_2), N_2O, NH_3 and C_3H_6 in the inlet and outlet gases were continually analyzed by an FT-IR (Antaris IGS, Thermo Fisher Scientific). The catalysts were pretreated in the simulated gases at 550 °C for 2 h before the activity test. Catalytic activity tests were carried out over the temperature range of 150-550 °C, and activity results were recorded after holding at each temperature for 50 min. The NO_x conversion and C_3H_6 conversion were calculated using the following formulas:

$$NO_x \text{ conversion } (\%) = \frac{([NO]in-[NO]out-[NO_2]out-2[N_2O]out)}{[NO]in} \times 100\ \% \quad (1)$$

$$C_3H_6 \text{ conversion } (\%) = \frac{[C_3H_6]in - [C_3H_6]out}{[C_3H_6]in} \times 100\ \% \quad (2)$$

$$NH_3 \text{ conversion } (\%) = \frac{[NH_3]in - [NH_3]out}{[NH_3]in} \times 100\ \% \quad (3)$$

2.3. Catalyst characterization

A QUADRASORB SI automatic surface analyzer system (Quantachrome Corporation) was used to measure the N_2 adsorption isotherms of the samples at the temperature of liquid N_2 (-196 °C). The specific surface areas were determined from the linear portion of the BET plot. Prior to the adsorption of N_2, the samples were evacuated at 300 °C for 6 h.

The chemical content of each sample was determined by inductively coupled plasma atomic emission spectrometry (ICP-AES) with an IRIS Intrepid II XSP apparatus (Thermo Fisher Scientific Ins).

XRD data were collected on a Rigaku D/MAX-rA diffractometer with Cu radiation (λ = 0.15406 nm). The X-ray tube was operated at 45 kV and 25 mA. The samples were investigated in the 2θ range of 5-50 ° at a scanning speed of 0.02 $°S^{-1}$.

UV-Vis-DRS were taken at room temperature on a "Shimadzu" UV-3600 PC spectrophotometer equipped with a diffuse reflectance accessory, and Barium sulfate was used in background scans. The test sample was the mixture of 250 mg of catalyst and 1000 mg of $BaSO_4$. Spectra were collected from 200 to 1100 nm.

The H_2-TPR was carried out on a commercial instrument with a TCD detector (Xianquan, TP5076), and 100 mg of sample was applied for each measurement. The sample was first pretreated in 5 % O_2/N_2 (30 ml/min) at 500 °C for 1 h to remove H_2O and other impurities adsorbed on the surface of the sample. Then, the sample was cooled to 50 °C in 5 % O_2/N_2 flow, the H_2-TPR was carried out at a linear heating rate of 5 °C/min from 50 °C to 900 °C under 5 vol. % H_2/N_2 (30 ml/min) flow.

NH_3-TPD was carried out on TP5076, and 100 mg of sample was applied for each measurement. The sample was first pretreated in He flow (30 ml/min) at 400 °C for 1 h to remove H_2O and other impurities adsorbed on the surface of the sample. Then, the sample was cooled to 120 °C, the catalyst was exposed in NH_3 (2% NH_3/N_2, 30ml/min) at 120 °C for 30 min, after that the catalyst was purged by He (30 ml/min) for 60 min to

remove physically adsorbed NH_3. Finally NH_3-TPD was performed at a linear heating rate of 10 °C/min from 120 to 650 °C under He flow (30 ml/min).

A TGA (Hengjiu) was conducted to determine the adsorption of C_3H_6 and C_3H_6/O_2 on various catalysts. The sample (10.0 mg) was first pretreated in N_2 for the adsorption test of C_3H_6 or 10 % O_2/N_2 (35ml/min) for the adsorption test of C_3H_6/O_2 at 400 °C for 1 h to remove H_2O and other impurities adsorbed on the surface of the sample. Then, the sample was cooled to the specified temperature in N_2 or 10 % O_2/N_2 flow and held for 15 min. Afterwards, 1% C_3H_6/N_2 (35 ml/min) was fed into the TGA reactor for propene adsorption test at 120 °C for 90 min, or the gas mixture (35 ml/min) containing 700 ppm C_3H_6, 8 % O_2 and N_2 as balance gas was fed into the TGA reactor until the saturation of the propene adsorption on the catalyst reached for 70 min for C_3H_6/O_2 adsorption test.

3. Results and discussion

3.1. Activity test

3.1.1. The NH_3-SCR performance of Cu and CuCe-x catalysts

The temperature dependence of NO_x conversion and N_2O formation during NH_3-SCR reaction over Cu and series of CuCe catalysts was presented in Fig. 1 a. All CuCe catalysts performed better NH_3-SCR activity than the Cu catalyst. In addition, the order of activities of these catalysts was as follows: CuCe-1.3 > CuCe-1.9 ~ CuCe-2.6 > Cu catalyst, and the T_{50} (T_{50} represented the temperature when NO_x conversion of catalyst

reached 50 %) of Cu, CuCe-1.3, CuCe-1.9 and CuCe-2.6 catalyst was 163, 151, 157 and 157 °C, respectively. In addition, the NH_3 oxidation performance of Cu and CuCe-x catalysts was shown in Fig. 1 b, it could be found that the addition of Ce could improve the NH_3 oxidation performance of Cu catalyst which may be unfavorable to the NH_3-SCR performance at high temperature. However, the NH_3-SCR performance of CuCe-x catalysts was higher than that of Cu catalyst. Thus, the NH_3-SCR activities of Ce catalysts and H-SAPO-34 support material were investigated and the results were shown in Fig. 1S. As can be seen therein, the addition of Ce could promote the NH_3-SCR activity at temperatures above 350 °C, suggesting that Ce could be the active sites above 350 °C and the better performance of CuCe-x catalysts above 350 °C was due to the addition of Ce. In addition, the addition of Ce did not significantly affect the activity at temperatures below 300 °C, inferring that Ce was not active sites of CuCe-x catalysts at low temperature. N_2O was not only a greenhouse gas which was much more serious than CO_2, but also an ozone depletion catalyst, so the generation of N_2O was one of important aspects in practical use to evaluate the performance of SCR catalyst and the results were also depicted in Fig.1. It could be found that extremely low amount of N_2O (< 3 ppm) was detected during activity tests over all catalysts and concentration of NO_2 was lower than 5 ppm in outlet (data not listed), indicating the high selectivity of NO_x to N_2. The results above indicated that the addition of Ce could improve the NH_3-SCR activity of Cu catalyst.

3. 1. 2. The effect of the concentration of C_3H_6 on the NH_3-SCR activity of Cu catalyst

The effect of the concentration of C_3H_6 on the NH_3-SCR activity of Cu catalyst was presented in Fig. 2 a. the NH_3-SCR performance of the Cu catalyst at temperatures below 400 °C decreased while C_3H_6 was added into the simulated gas. It could be found that the NO_x conversion increased as the temperature increasing below 250 °C, then decreased in the range of 250-300 °C, afterwards the NO_x conversion further increased with the temperature increasing, until it reached 400 °C, finally, the NO_x conversion decreased as the temperature increasing above 400 °C, and an M-shaped curve was formed. In addition, the extent of the decrease of NH_3-SCR activity increased as the concentration of C_3H_6 increasing, inferring that the poisoning of Cu catalyst by C_3H_6 was related to the concentration of C_3H_6 which was consistent with the results in the literatures. [5, 13] HCs resistance of the NH_3-SCR catalyst was influenced by HCs oxidation property,[5] herein, the C_3H_6 oxidation performance in oxidation atmosphere (simulated gas without NH_3 and NO) and in simulated exhaust gas was tested and shown in Fig. 2 c and Fig. 2 d, respectively. Luo et al. [14] demonstrated that the formation of oxidized intermediates through incomplete oxidation of C_3H_6 would decrease the NH_3-SCR activity of Cu catalyst. It could be found that the C_3H_6 conversion of Cu catalyst was near zero at 250 °C, and increased sharply from 300 to 400 °C as shown in Fig. 2 c and Fig. 2 d, so that M-shaped NO_x conversion curve was obtained. Meanwhile, the C_3H_6 conversion in oxidation atmosphere or in simulated exhaust gas of Cu catalyst decreased with the concentration of C_3H_6 increasing, combined with the poisoning results of NH_3-SCR performance, it could be speculated that the catalyst with better C_3H_6 oxidation activity may suppress the formation of

intermediates, thus, the catalyst with better C_3H_6 conversion performed better NH_3-SCR activity. Meanwhile, it could be found that the NH_3-SCR performance of Cu catalyst was also inhibited at low temperature range. As C_3H_6 oxidation activity was near zero, and less coke or stable intermediates was formed, and it could be found that the inhibition effect on Cu catalyst increased with the concentration of C_3H_6 increasing. Thus, the competitive adsorption between C_3H_6 and NO_x would inhibit the NH_3-SCR performance of Cu catalyst which has been confirmed by Ma et al. [19] In contrast, the addition of C_3H_6 did not significantly affect the NH_3-SCR activity of Cu catalyst at temperatures above 400 °C. The HC-SCR activity of the Cu catalyst was also tested, and the results were shown in Fig. 2 b. It could be found that the HC-SCR reaction mainly happened between 350 and 550 °C, and the NO_x conversion increased as the concentration of C_3H_6 increasing. Indeed, at the temperature above 350 °C, the increase extent of NO_x conversion did not change obviously after the addition of C_3H_6. Heo et al. [13] reported that NH_3 could be partially consumed by C_3H_6, thus, HC-SCR, NH_3-SCR and NH_3 consumption took place simultaneously, leading to little changes of the NO_x conversions above 400 °C.

3. 1. 3. The effect of C_3H_6 on the NH_3-SCR of Cu and CuCe catalyst

To compare the HCs resistance of the Cu and CuCe-x catalysts, 700 ppm of C_3H_6 was introduced into the NH_3-SCR simulated gas feed. The effect of C_3H_6 on the NH_3-SCR of Cu and CuCe-x catalysts was shown in Fig. 3 a. It could be found that at temperatures below 400 °C (LT) the NH_3-SCR performance of all the catalysts

decreased with the addition of C_3H_6, and the NO_x conversion of the Cu and CuCe-x catalysts did not change obviously at temperatures above 400 °C (HT). In addition, CuCe-x catalysts performed higher NO_x conversions than Cu catalyst, the order of activities of these catalysts at LT was as follows: CuCe-1.9 > CuCe-1.3 > CuCe-2.6 > Cu catalyst, the order of activities at HT was as follows: CuCe-1.3 ~ CuCe-2.6 > Cu ~ CuCe-1.9 catalyst. Furthermore, the HC-SCR performance of the Cu and CuCe-x catalysts was displayed in Fig. 3 b, the NO_x conversion increased from 300 to 350 °C, and kept stable at temperatures between 350 and 500 °C, then slightly decreased at 550 °C. The order of NO_x conversion of CuCe-x catalysts was as follows: CuCe-1.3 > CuCe-2.6 > CuCe-1.9. At HT, the trend of the HC-SCR of CuCe-x catalysts was the same with that of the NH_3-SCR with C_3H_6, and the NH_3-SCR performance of CuCe-x catalysts was similar, inferring that the HC-SCR slightly improved the NO_x conversion of CuCe-x catalysts with the addition of C_3H_6 at HT. Moreover, since the catalyst with better C_3H_6 oxidation activity would perform better HCs resistance, [5] the C_3H_6 oxidation performance of the Cu and CuCe-x catalysts was investigated, and the results were shown in Fig. 3 c and Fig. 3 d. The C_3H_6 conversion of the CuCe-x catalysts was higher than that of Cu catalyst, thus, the HCs resistance of CuCe-x catalysts was better than that of Cu catalyst. In addition, the order of C_3H_6 conversion of CuCe-x catalysts decreased as follows: CuCe-1.3 ≥ CuCe-1.9 ≥ CuCe-2.6. It could be found that the C_3H_6 conversion of CuCe-1.3 was slightly higher than that of CuCe-1.9 at 300 °C, while the HCs resistance of CuCe-1.9 was better than that of CuCe-1.3 at 300 °C. Luo et al. [14] reported that the stable intermediate species formed during C_3H_6 oxidation

would inhibit the NO_x conversion. Reaction between C_3H_6 and O_2 would generate stable intermediate species in the channel of the catalysts, and the amount of stable intermediate species may influence the NH_3-SCR activity more seriously, more details were shown in section 3.6.

3. 2. Textural and structural properties of Cu and CuCe-x catalysts.

The surface areas and pore structure results of H-SAPO-34 and the catalysts were summarized in Table 1. The surface areas and pore volumes of SAPO-34 decreased slightly after Cu and/or Ce were impregnated. According to the literatures, part of the copper and/or cerium species migrated into the channel of zeolite, which blocked part of the channel of zeolite and consequently caused the decrease of the textural property of zeolite. [39, 40] Thus, it was understandable that the surface areas of the catalysts gradually reduced as the amount of cerium increasing. Furthermore, the effects of the addition of Ce on the structure of copper species in Cu-containing catalysts were examined by XRD measurements (Fig. 4). All the patterns in Fig. 4 showed diffraction peaks typical of SAPO-34 structure. In addition, the CeO_2 and/or Ce_2O_3 phase cannot be identified in the XRD patterns of CuCe-x catalysts, suggesting that the Ce species were dispersed well or too small to be detected. Furthermore, two peaks at 35.55 ° and 38.73 ° which were corresponded to the CuO phase (PDF, 48-1548) could be observed in XRD spectra. The CuO formed by the aggregation of extra-copper species on the surface of SAPO-34. Moreover, the intensities of the peaks of CuO phase decreased significantly after the addition of Ce, inferring that the amount of CuO species in

Cu-SAPO-34 was higher than those in CuCe-x catalysts, and the average crystallite sizes of CuO of Cu and CuCe-x catalysts were calculated based on the Sherrer equation (Table 1), it could be found that the average crystallite sizes of CuO of CuCe-x catalysts were smaller than that of Cu catalyst, indicating that the addition of Ce could decrease the amount of CuO species and inhibit the growth of CuO clusters.

3. 3. Nuclearity of the Cu and Ce species

UV–vis DRS was used to identify the nuclearity of the Cu and Ce species in the catalysts. Fig. 5 showed the UV-vis DRS of the Cu catalyst and CuCe catalysts with various contents of Ce. As reported in the literatures, for Cu species, the absorption band centered at 226 nm was attributed to charge transitions from $O_{zeolite}$ to isolated Cu^{+}/Cu^{2+} ions, [41-44] the bands at 349 and 468 nm were assigned to O–Cu–O and Cu–O–Cu complex, [41] respectively, and the band from 650 to 800 nm was attributed to d-orbitals electronic transitions of Cu^{2+} in CuO clusters. [41, 43, 45] In addition, for Ce species, the absorption band at 301 nm was attributed to the charge transitions from O to Ce^{4+} species in CeO_2 clusters of several nanometers in size. [46, 47]

It could be found that four types of absorption bands which located at 226, 349, 468 and 600-800 nm existed in the spectrum of Cu catalyst in Fig. 5. In addition, for CuCe catalysts, a band at 301 nm appeared, the intensity of which increased with the content of Ce increasing, suggesting that the content of CeO_2 clusters increased with the content of Ce increasing. The recorded UV-vis-DRS were de-convoluted into sub-bands by applying Gauss functions, and the isolated copper species, O-Cu-O, Cu-O-Cu and CuO clusters were semi-estimated relative to each other by the area ratios

of the different sub-bands. And the semi-quantified results were shown in Table 2. Furthermore, it could be found that the relative concentrations of CuO cluster of CuCe-x catalysts decreased significantly compared with that of Cu catalyst, and the ICP-AES results showed that the copper content of Cu catalyst was similar with those of CuCe-x catalysts, indicating that the addition of Ce could inhibit the generation of CuO species which was consistent with the XRD results. Meanwhile, the relative concentrations of isolated Cu^{+}/Cu^{2+} at 226 nm increased as follows: Cu < CuCe-2.6 ≤ CuCe-1.3 ≤ CuCe-1.9. Thus, it could be inferred that the amount of isolated copper ions increased distinctly with the addition of Ce, and the isolated Cu^{+}/Cu^{2+} was recognized as the active sites of Cu-SAPO-34. [25, 26] Therefore, the activity of CuCe-x catalysts was better that that of Cu catalyst.

3. 4. H_2-TPR test

H_2-TPR was applied to identify the copper species in the catalysts. The H_2-TPR results of Cu and CuCe-x catalysts were depicted in Fig. 6. For all catalysts, a sharp peak (200-350 °C) and a broad peak (350-500 °C) could be found in the H_2-TPR profiles. The sharp peak could be de-convoluted into three peaks (A, B and C) due to its asymmetry. Peak A at around 225 °C was assigned to the reduction of Cu^{2+} in CHA cage (Cu^{2+} to Cu^{+}), [12, 48, 49] peak B at around 265 °C was assigned to the reduction of CuO to Cu^{0}, [50] peak C at around 312 °C was assigned to the reduction of Cu^{2+} on D6R in the sodalite cage to Cu^{+} [12, 48, 49] and the broad peak D could be assigned to the reduction of Cu^{+} to Cu^{0} and/or Ce^{4+} to Ce^{3+}. [48] In addition, the amounts of isolated Cu^{2+}

ions of Cu and CuCe-x catalysts were estimated by H_2-TPR measurement, and results were listed in Table 3. It could be found that the amount of CuO species of Cu catalyst was larger than those of CuCe-x catalysts, which was consistent with the XRD measurement. In addition, the amounts of isolated copper species of CuCe-x catalysts were higher than that of Cu catalyst which were consistent with the results of UV-vis DRS, thus, the NH_3-SCR performance of CuCe-x catalysts was better than that of Cu catalyst.

3.5. Acidity of Cu and CuCe-x catalysts

As Lin et al. [23] reported that coking occurred preferentially on strong acid sites, and the acid property of the Cu-SAPO-34 was very important for NH_3-SCR performance, [51-53] NH_3-TPD was applied to determine the effect of the addition of Ce on the acid property of Cu-SAPO-34. Fig. 7 showed the NH_3-TPD profiles of H-SAPO-34 support material, Cu and CuCe-x catalysts. The NH_3-TPD profile of the support material contained two distinguishable regions which could be de-convoluted into four peaks located at ca. 195 (A), 273 (B), 375 (C) and 440 °C (D), respectively. According to the literatures, the peak (A) at lower temperature was assigned to the weak Brønsted acid sites at surface hydroxyls, [52, 54] and the peaks (B, C and D) at higher temperatures were related to the structural Brønsted acid sites referred to moderate (B) and strong acidity (C and D). [7, 55, 56] Two peaks located at 353 and 545 °C were observed in the NH_3-TPD profile of Cu and CuCe-x catalyst. The former (C) was ascribed to NH_3 desorbed form the structural Brønsted acid sites and overlapped with NH_3 desorbed from the acid sites created by

CuO fine particles and/or Cu–O–Cu clusters interact with SAPO-34, and the latter (E) was ascribed to NH_3 desorbed from the strong Lewis sites created by copper species. [37] Meanwhile, compared with the support material peak A of Cu and CuCe-x catalysts was ascribed to the weak Brønsted acid sites and weak Lewis acid sites related to Cu and/or Ce, [52, 55] and peak D of Cu and CuCe-x catalysts was assigned to strong Brønsted acid sites created by SAPO-34 and Lewis acid sites related to Cu and/or Ce species. [52, 55] Furthermore, the amount of acid was calculated by integration of the areas of NH_3-TPD profiles, and the results were displayed in Table 4. It could be found that the amounts of acid of CuCe-x catalysts were lower than that of Cu catalyst. In this study, although the total amount of acid sites decreased, the NH_3-SCR performance of CuCe-x catalysts was not affected, this may be due to the increased amount of the active sites (isolated copper ions) which compensated the negative effect of the decrease of the amount of acid sites on the NH_3-SCR performance. In addition, the amounts of strong acid sites of CuCe-x catalysts were lower than that of Cu catalyst. Furthermore, compared with the profile of Cu catalyst, the desorption of NH_3 from strong acid sites (C and D) of CuCe-x catalysts shifted to lower temperatures, and the temperatures of peak C and peak D of CuCe-x catalysts decreased by 13 and 8 °C, respectively, inferring that the addition of Ce could reduce the acid strength of strong acid sites. It could be concluded that the addition of Ce not only decreased the amount of strong acid sites but also decreased the acid strength of strong acid sites. Therefore, the coke deposit may be inhibited by the addition of Ce.

3.6. The C_3H_6/O_2 adsorption property of Cu and CuCe-x catalysts

To investigate the C_3H_6/O_2 adsorption process over Cu and CuCe catalysts, C_3H_6/O_2 adsorption on the catalysts was measured at 200, 300 and 400 °C by TGA, and the results were shown in Fig. 8. It could be seen that the amount of adsorption of C_3H_6/O_2 decreased as the temperature increasing, and there was almost no C_3H_6 adsorption on the catalysts at 400 °C which was consistent with the results that C_3H_6 was nearly completely conversed at temperatures above 400 °C. Therefore, the addition of C_3H_6 did not inhibit the NH_3-SCR performance of the Cu and CuCe-x catalysts at HT. Ma et al. [19] confirmed that the competitive adsorption of NO_x and C_3H_6 would reduce the activity of Cu-SSZ-13 catalyst at low temperature range. The adsorbed amount of C_3H_6/O_2 on Cu catalyst was higher than those on CuCe-x catalysts at 200 °C, thus the NH_3-SCR performance of CuCe-x catalysts with lower C_3H_6 adsorption property was better than that of Cu catalyst at low temperature. In addition, the adsorbed amount of C_3H_6/O_2 on Cu catalyst was significantly higher than those on CuCe-x catalysts at 300 °C. At 300 °C, the adsorbed C_3H_6 could transform to coke on the strong acid sites of the catalysts by uncompleted oxidizing of C_3H_6, the formed coke could block the pores of SAPO-34 and even cover the active sites of the catalysts to degrade the NH_3-SCR performance of the Cu and CuCe-x catalysts, and the results listed in Table 4 showed that the CuCe-x catalysts owned lower amounts of strong acid sites, thus, the CuCe-x catalysts with lower amounts of adsorbed C_3H_6 performed better NO_x conversion activity. In addition, it should be noted that the adsorbed amount of propene of CuCe-1.3 catalyst was higher than that of CuCe-1.9, thus, although the C_3H_6

conversion of CuCe-1.3 was higher than that of CuCe-1.9 catalyst, the NO_x conversion of CuCe-1.9 was better than that of CuCe-1.3 catalyst in the presence of C_3H_6.

4. Conclusion:

The NH_3-SCR activity and HCs poisoning behavior of Cu and CuCe-x catalysts were explored in this study. Since ceria could undergo NH_3-SCR process at high temperature, the addition of Ce could improve the NH_3-SCR performance of Cu catalyst at high temperature. The XRD results showed that the crystallite sizes of CuO of CuCe-x catalysts were smaller than that of Cu catalyst. In addition the H_2-TPR results revealed that the amounts of CuO species in CuCe-x catalysts were lower than that in Cu catalyst. Furthermore, H_2-TPR and UV-vis-DRS results indicated that the amounts of isolated copper species which was demonstrated as the active sites of Cu-SAPO-34 in CuCe-x catalysts were higher than that in Cu catalyst. Thus, it could be concluded that the introduction of Ce could efficiently promote the dispersion of copper species, create larger amount of isolated copper ions and inhibit the aggregation of the CuO species. Therefore, the addition of Ce improved the activity of the Cu catalyst.

The NH_3-SCR activity of Cu and CuCe-x catalysts was inhibited by C_3H_6 poisoning, and the extent of inhibition increased with the concentration of C_3H_6 increasing. CuCe-x catalysts performed better C_3H_6 oxidation than Cu catalyst, indicating that the addition of Ce could decrease the concentration of C_3H_6 in simulated gas feed. The NH_3-TPD results showed that the strength and amount of the strong acid sites of CuCe-x catalysts were lower than those of Cu catalyst. In addition, the TGA results

showed that the amounts of C_3H_6/O_2 adsorption on the CuCe-x catalysts were smaller than that on the Cu catalyst. It could be concluded that the addition of Ce could inhibit the C_3H_6 adsorption. Therefore, it could be concluded that the addition of Ce could improve the HCs resistance of Cu-SAPO-34 catalyst.

Acknowledgements

This work was financially supported by the National Natural Science Foundation of China (Grant No. 21173153), the National High-Tech Research and Development (863) Program of China (Grant No. 2013AA065304). The authors gratefully acknowledge Yu Hao and Xiaomeng Luo (Sichuan University) for their help with activity test.

Reference:

1. R.-J. Huang, Y. Zhang, C. Bozzetti, K.-F. Ho, J.-J. Cao, Y. Han, K. R. Daellenbach, J. G. Slowik, S. M. Platt, F. Canonaco, P. Zotter, R. Wolf, S. M. Pieber, E. A. Bruns, M. Crippa, G. Ciarelli, A. Piazzalunga, M. Schwikowski, G. Abbaszade, J. Schnelle-Kreis, R. Zimmermann, Z. An, S. Szidat, U. Baltensperger, I. E. Haddad and A. S. H. Prevot, *Nature*, 2014, 514, 218-222.
2. P. Granger and V. I. Parvulescu, *Chem. Rev.*, 2011, 111, 3155-3207.
3. L. Xie, F. Liu, L. Ren, X. Shi, F.-S. Xiao and H. He, *Environ. Sci. Technol.*, 2013, 48, 566-572.
4. M. Fu, C. Li, P. Lu, L. Qu, M. Zhang, Y. Zhou, M. Yu and Y. Fang, *Catal. Sci. Technol.*, 2014, 4, 14-25.
5. Y. J. Kim, H. J. Kwon, I. Heo, I.-S. Nam, B. K. Cho, J. W. Choung, M.-S. Cha and G. K. Yeo, *Appl. Catal. B: Environ.*, 2012, 126, 9-21.
6. H. Y. Huang, R. Q. Long and R. T. Yang, *Appl. Catal. A: Gen*, 2002, 235, 241-251.
7. L. Ma, Y. Cheng, G. Cavataio, R. W. McCabe, L. Fu and J. Li, *Appl. Catal. B: Environ.*, 2014, 156–157, 428-437.
8. G. Cavataio, J. Girard, J. E. Patterson, C. Montreuil, Y. Cheng and C. K. Lambert, *SAE International*, 2007, 01, 1575.
9. J. H. Kwak, R. G. Tonkyn, D. H. Kim, J. Szanyi and C. H. F. Peden, *J. Catal.*, 2010, 275, 187-190.

10. J. H. Kwak, D. Tran, S. D. Burton, J. Szanyi, J. H. Lee and C. H. F. Peden, *J. Catal.*, 2012, 287, 203-209.
11. D. W. Fickel, E. D'Addio, J. A. Lauterbach and R. F. Lobo, *Appl. Catal. B: Environ.*, 2011, 102, 441-448.
12. L. Ma, Y. Cheng, G. Cavataio, R. W. McCabe, L. Fu and J. Li, *Chem. Eng. J.*, 2013, 225, 323-330.
13. I. Heo, Y. Lee, I.-S. Nam, J. W. Choung, J.-H. Lee and H.-J. Kim, *Microporous Mesoporous Mater.*, 2011, 141, 8-15.
14. J.-Y. Luo, H. Oh, C. Henry and W. Epling, *Appl. Catal. B: Environ.*, 2012, 123–124, 296-305.
15. P. G. Blakeman, E. M. Burkholder, H.-Y. Chen, J. E. Collier, J. M. Fedeyko, H. Jobson and R. R. Rajaram, *Catal. Today*, 2014, 231, 56-63.
16. T. Ishihara, M. Kagawa, F. Hadama and Y. Takita, *J. Catal.*, 1997, 169, 93-102.
17. B. J. Adelman, T. Beutel, G. D. Lei and W. M. H. Sachtler, *J. Catal.*, 1996, 158, 327-335.
18. M. Hyeon Kim, U.-C. Hwang, I.-S. Nam and Y. Gul Kim, *Catal. Today*, 1998, 44, 57-65.
19. L. Ma, W. Su, Z. Li, J. Li, L. Fu and J. Hao, *Catal. Today*, 2015, 245, 16-21.
20. C.-K. Seo, B. Choi, H. Kim, C.-H. Lee and C.-B. Lee, *Chem. Eng. J.*, 2012, 191, 331-340.
21. J. Li, R. Zhu, Y. Cheng, C. K. Lambert and R. T. Yang, *Environ. Sci. Technol.*, 2010, 44, 1799-1805.
22. Q. Ye, L. Wang and R. T. Yang, *Appl. Catal. A: Gen*, 2012, 427–428, 24-34.
23. X. Lin, Y. Fan, G. Shi, H. Liu and X. Bao, *Energy Fuels*, 2007, 21, 2517-2524.
24. L. Ma, J. Li, Y. Cheng, C. K. Lambert and L. Fu, *Environ. Sci. Technol.*, 2012, 46, 1747-1754.
25. L. Wang, W. Li, G. Qi and D. Weng, *J. Catal.*, 2012, 289, 21-29.
26. J. Xue, X. Wang, G. Qi, J. Wang, M. Shen and W. Li, *J. Catal.*, 2013, 297, 56-64.
27. S. J. Schmieg, S. H. Oh, C. H. Kim, D. B. Brown, J. H. Lee, C. H. F. Peden and D. H. Kim, *Catal. Today*, 2012, 184, 252-261.
28. I. Lezcano-Gonzalez, U. Deka, H. E. van der Bij, P. Paalanen, B. Arstad, B. M. Weckhuysen and A. M. Beale, *Appl. Catal. B: Environ.*, 2014, 154–155, 339-349.
29. A. Sultana, T. Nanba, M. Haneda and H. Hamada, *Catal. Commun.*, 2009, 10, 1859-1863.
30. F. Gao, J. Kwak, J. Szanyi and C. F. Peden, *Top. Catal.*, 2013, 56, 1441-1459.
31. M. S. Avila, C. I. Vignatti, C. R. Apesteguía and T. F. Garetto, *Chem. Eng. J.*, 2014, 241, 52-59.
32. H.-J. Sedjame, C. Fontaine, G. Lafaye and J. Barbier Jr, *Appl. Catal. B: Environ.*, 2014, 144, 233-242.
33. Z. Lian, F. Liu and H. He, *Catal. Sci. Technol.*, 2014, 5, 389-396.
34. S. Yang, Y. Guo, H. Chang, L. Ma, Y. Peng, Z. Qu, N. Yan, C. Wang and J. Li, *Appl. Catal. B: Environ.*, 2013, 136–137, 19-28.

35. W. Shan, F. Liu, H. He, X. Shi and C. Zhang, *Appl. Catal. B: Environ.*, 2012, 115–116, 100-106.
36. H. Xu, Q. Zhang, C. Qiu, T. Lin, M. Gong and Y. Chen, *Chem. Eng. Sci.*, 2012, 76, 120-128.
37. Y. Cao, S. Zou, L. Lan, Z. Yang, H. Xu, T. Lin, M. Gong and Y. Chen, *J. Mol. Catal. A: Chem*, 2015, 398, 304-311.
38. Z. Yang, N. Zhang, Y. Cao, M. Gong, M. Zhao and Y. Chen, *Catal. Sci. Technol.*, 2014, 4, 3032-3043.
39. F. Bin, X. Wei, B. Li and K. S. Hui, *Appl. Catal. B: Environ.*, 2015, 162, 282-288.
40. F. Bin, C. Song, G. Lv, J. Song, S. Wu and X. Li, *Appl. Catal. B: Environ.*, 2014, 150–151, 532-543.
41. L. Wang, J. R. Gaudet, W. Li and D. Weng, *J. Catal.*, 2013, 306, 68-77.
42. S. A. Bates, A. A. Verma, C. Paolucci, A. A. Parekh, T. Anggara, A. Yezerets, W. F. Schneider, J. T. Miller, W. N. Delgass and F. H. Ribeiro, *J. Catal.*, 2014, 312, 87-97.
43. N. Wilken, R. Nedyalkova, K. Kamasamudram, J. Li, N. Currier, R. Vedaiyan, A. Yezerets and L. Olsson, *Top. Catal.*, 2013, 56, 317-322.
44. A. Shishkin, H. Kannisto, P.-A. Carlsson, H. Harelind and M. Skoglundh, *Catal. Sci. Technol.*, 2014, 4, 3917-3926.
45. H. Praliaud, S. Mikhailenko, Z. Chajar and M. Primet, *Appl. Catal. B: Environ.*, 1998, 16, 359-374.
46. Z. Li and M. Flytzani-Stephanopoulos, *J. Catal.*, 1999, 182, 313-327.
47. L. Yuliati, T. Hamajima, T. Hattori and H. Yoshida, *Chem. Commun.*, 2005, DOI: 10.1039/B507698F, 4824-4826.
48. Y. J. Kim, J. K. Lee, K. M. Min, S. B. Hong, I.-S. Nam and B. K. Cho, *J. Catal.*, 2014, 311, 447-457.
49. J. Hun Kwak, H. Zhu, J. H. Lee, C. H. F. Peden and J. Szanyi, *Chem. Commun.*, 2012, 48, 4758-4760.
50. F. Gao, E. D. Walter, N. M. Washton, J. Szanyi and C. H. F. Peden, *Appl. Catal. B: Environ.*, 2015, 162, 501-514.
51. T. Yu, J. Wang, M. Shen and W. Li, *Catal. Sci. Technol.*, 2013, 3, 3234-3241.
52. D. Wang, L. Zhang, K. Kamasamudram and W. S. Epling, *ACS catal.*, 2013, 3, 871-881.
53. T. Yu, J. Wang, M. Shen, J. Wang and W. Li, *Chem. Eng. J.*, 2015, 264, 845-855.
54. C. Petitto and G. Delahay, *Chem. Eng. J.*, 2015, 264, 404-410.
55. J. Wang, T. Yu, X. Wang, G. Qi, J. Xue, M. Shen and W. Li, *Appl. Catal. B: Environ.*, 2012, 127, 137-147.
56. T. Yu, D. Fan, T. Hao, J. Wang, M. Shen and W. Li, *Chem. Eng. J.*, 2014, 243, 159-168.

Captions for Tables

Table 1 The chemical composition, surface areas, pore volumes and CuO crystallite sizes of the catalysts.

Table 2 Relative concentrations of isolated copper ions, O-Cu-O, Cu-O-Cu and CuO clusters.

Table 3 Quantitative analysis of the H_2-TPR profiles of Cu and CuCe-x catalysts

Table 4 Acidity and the adsorption of propene of H-SAPO-34, Cu and CuCe-x catalysts.

Table 1

sample	Chemical composition of the catalyst [a] (wt%)					Surface areas (m^2/g)	Pore volumes (ml/g)	CuO crystallite size (nm) [b]
	Cu	Ce	Al	Si	P			
H-SAPO-34	-	-	-	-	-	603.2	0.26	-
Cu	3.0	-	19.8	3.2	17.3	583.5	0.26	31
CuCe-1.3	3.0	1.3	20.2	2.9	18.2	579.2	0.26	21
CuCe-1.9	3.0	1.9	19.2	3.1	17.4	555.4	0.25	21
CuCe-2.6	3.1	2.6	21.1	3.3	17.3	541.7	0.25	20

[a] analyzed by ICP-AES

[b] calculated by the Sherrer equation

Table 2

Sample	Relative concentrations of each species (%)			
	Isolated Cu^{+}/Cu^{2+}	O-Cu-O	Cu-O-Cu	CuO clusters
Cu	34.6	10.8	19.7	36.9
CuCe-1.3	42.4	12.8	24.2	22.6
CuCe-1.9	42.8	12.2	21.0	24.0
CuCe-2.6	41.2	1.1	22.4	24.3

Table 3

	H_2 consumption (μmol/g)	
Sample	Isolated Cu^{2+} ions (A + C)	CuO species (B/2)
Cu	203	218
CuCe-1.3	297	172
CuCe-1.9	281	185
CuCe-2.6	279	191

Table 4

Sample	The acid amount (mmol/g)				The amount of adsorption of propene (mmol/g) [a]
	Weak (A)	Moderate (B)	Strong acid (C + D + E)	Total	
H-SAPO-34	0.12	0.08	0.36	0.56	1.2
Cu	0.18	0.07	0.56	0.81	1.1
CuCe-1.3	0.15	0.09	0.50	0.74	0.97
CuCe-1.9	0.16	0.11	0.45	0.72	0.94
CuCe-2.6	0.14	0.10	0.49	0.73	1.0

[a] tested by TGA at 120 °C

Captions for Fig.

Fig. 1 The NO_x conversion and N_2O generation of Cu and CuCe-x catalysts (a), and NH_3 oxidation performance of Cu and CuCe-x catalysts (b). Feed condition: 350 ppm of NH_3, 350 ppm of NO, 8% of O_2, 5 vol% of H_2O (a), 350 ppm of NH_3, 8% of O_2, 5 vol% of H_2O (b) and N_2 balance, GSHV: 30,000 h^{-1}.

Fig. 2 Effect of C_3H_6 concentrations on the NH_3-SCR performance (a), HC-SCR performance (b), C_3H_6 oxidation performance in oxidation atmosphere (c) and C_3H_6 oxidation performance in simulated exhaust gas (d) of Cu catalyst. Feed condition: 350 ppm of NH_3, 350 ppm of NO, 8% O_2, 5 vol% H_2O, 350–1050 ppm of C_3H_6 (a, d), 350 ppm of NO, 8% O_2, 5 vol% H_2O, 350–1050 ppm of C_3H_6 (b), 8% O_2, 5 vol% H_2O, 350–1050 ppm of C_3H_6 (c), and N_2 balance, GSHV: 30,000 h^{-1}.

Fig. 3 the NH_3-SCR performance (a), HC-SCR performance (b), C_3H_6 oxidation performance in oxidation atmosphere (c) and C_3H_6 oxidation performance in simulated exhaust gas (d) of Cu and CuCe-x catalysts. Feed condition: 350 ppm of NH_3, 350 ppm of NO, 8% O_2, 5 vol% H_2O, 700 ppm of C_3H_6 (a, d), 350 ppm of NO, 8% O_2, 5 vol% H_2O, 700 ppm of C_3H_6 (b), 8% O_2, 5 vol% H_2O, 700 ppm of C_3H_6 (c), and N_2 balance, GSHV: 30,000 h^{-1}.

Fig. 4 XRD patterns of the Cu and CuCe-x catalysts.

Fig. 5 UV-vis-DRS of the Cu and CuCe-x catalysts.

Fig. 6 H_2-TPR profiles of Cu and CuCe-x catalysts.

Fig. 7 NH_3-TPD profiles of Cu and CuCe-x catalysts.

Fig. 8 C_3H_6 adsorption on the catalysts at 200, 300, and 400 °C, respectively. Feed

condition: 700 ppm of C_3H_6, 8 % of O_2 and balanced by N_2, feed flow: 35 ml/min.

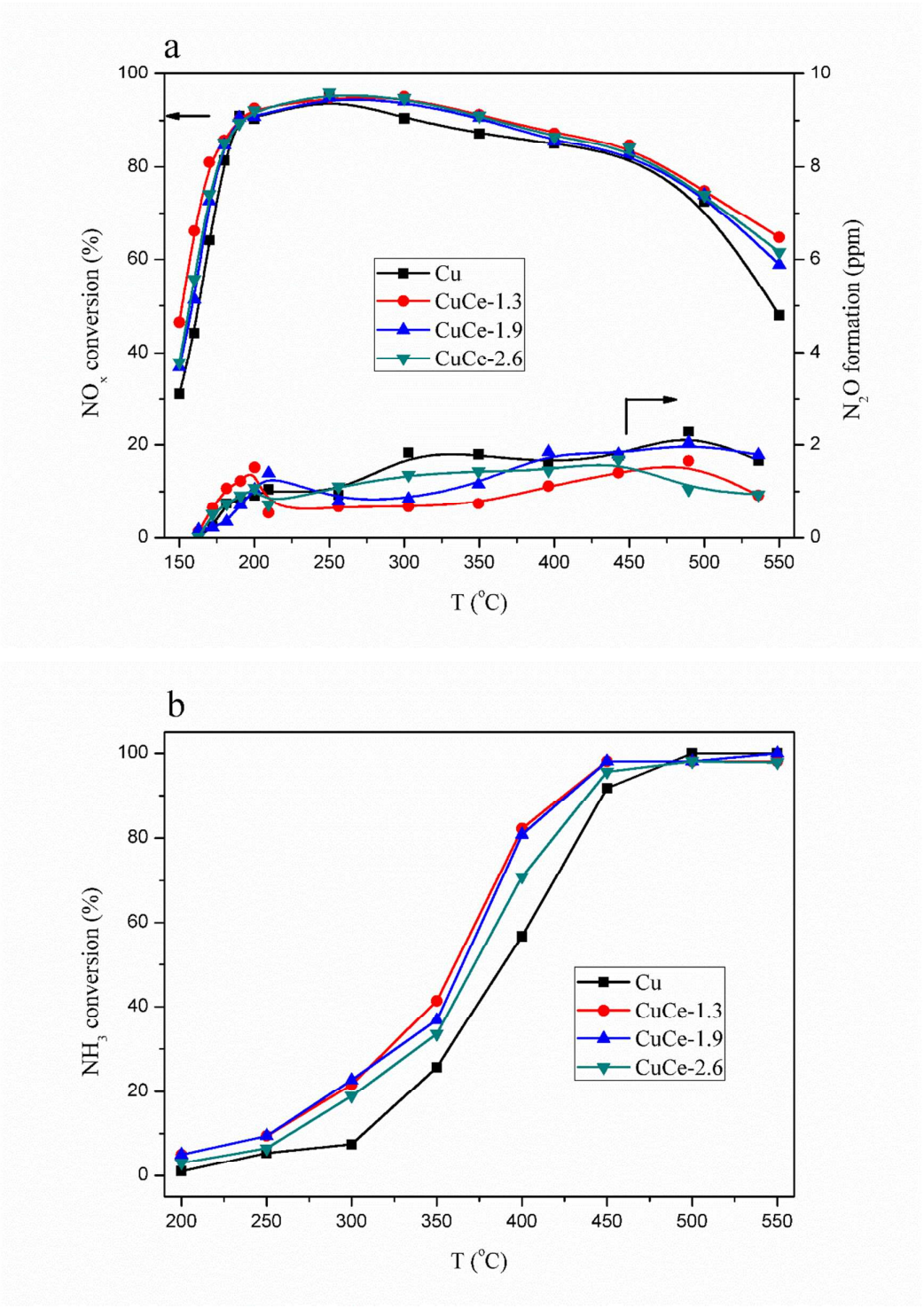

Fig.1

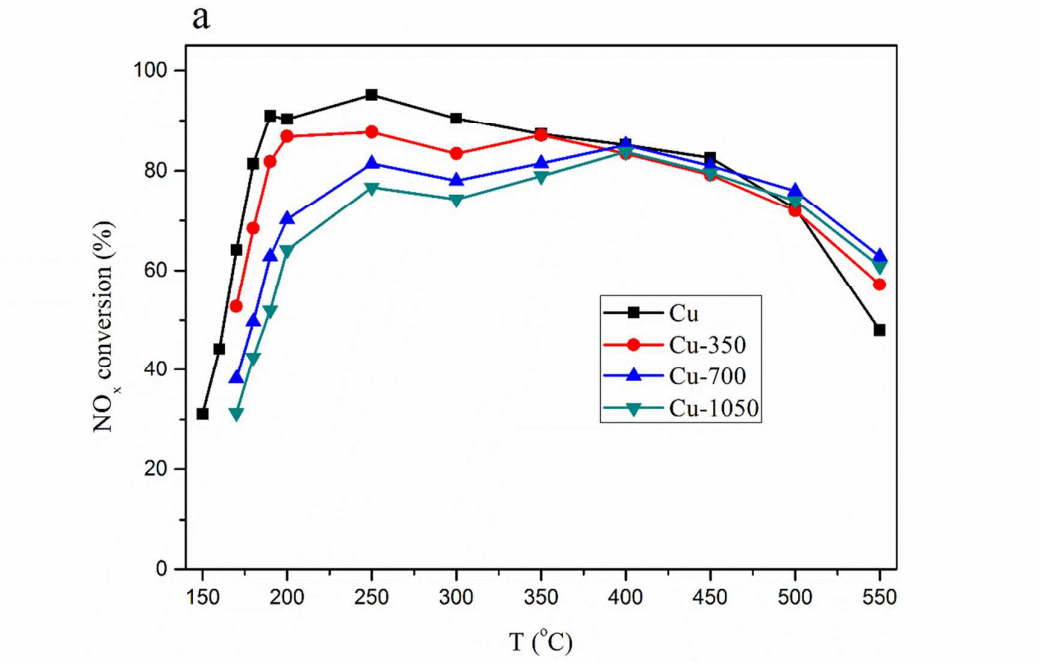

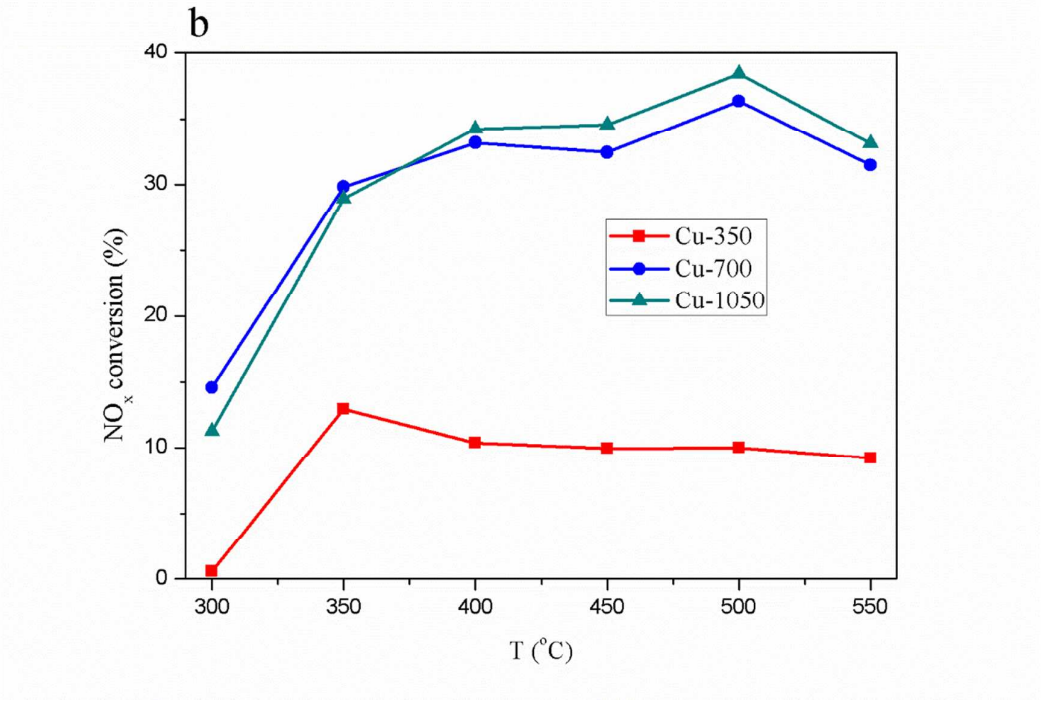

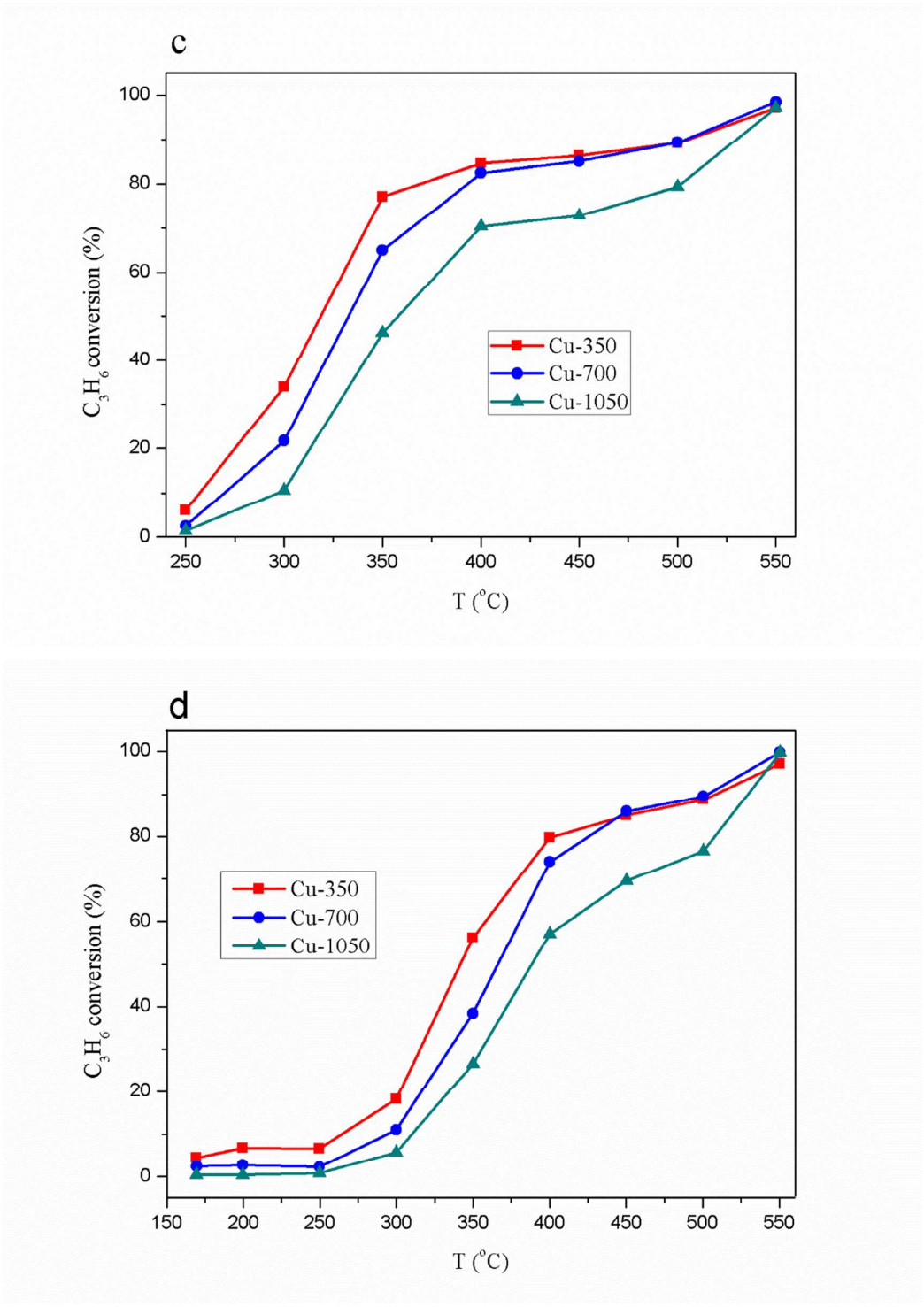

Fig. 2

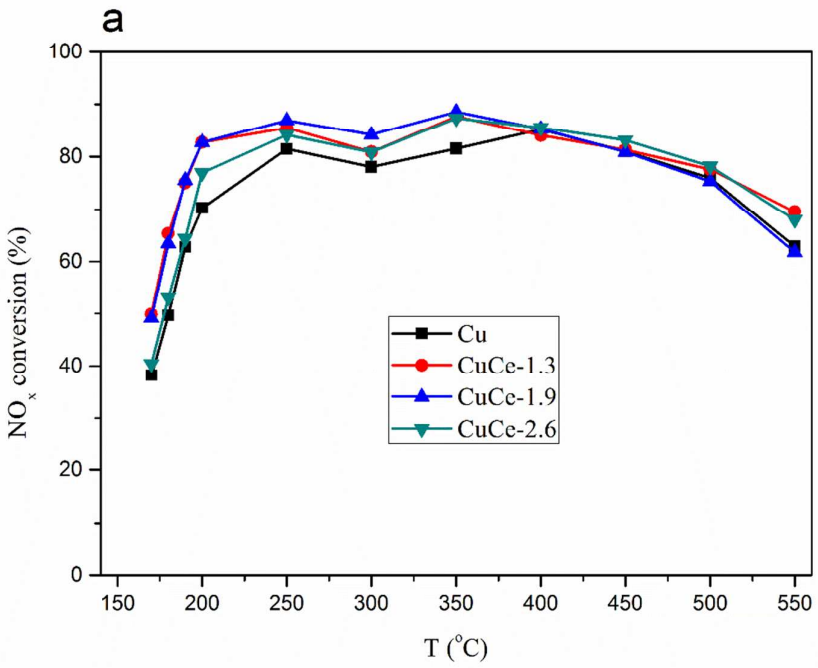

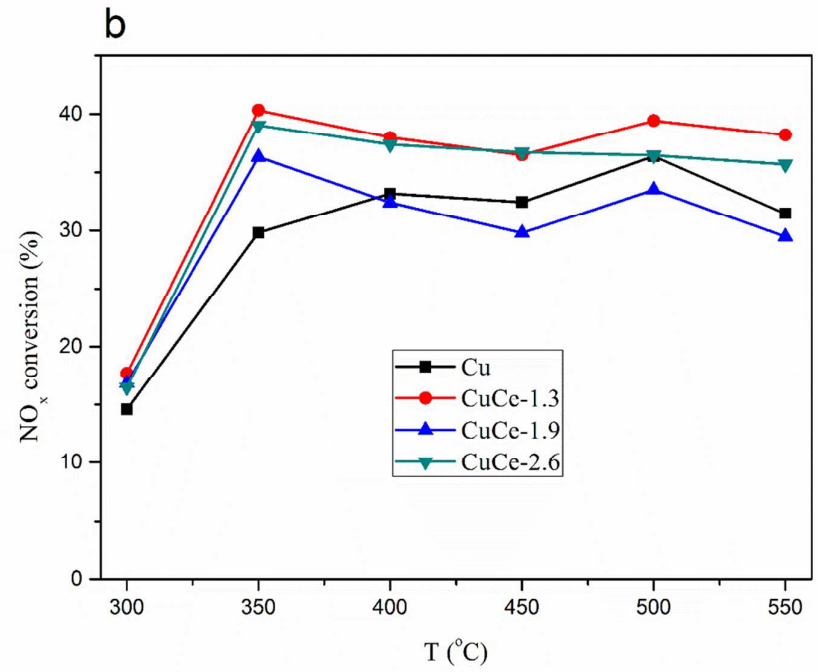

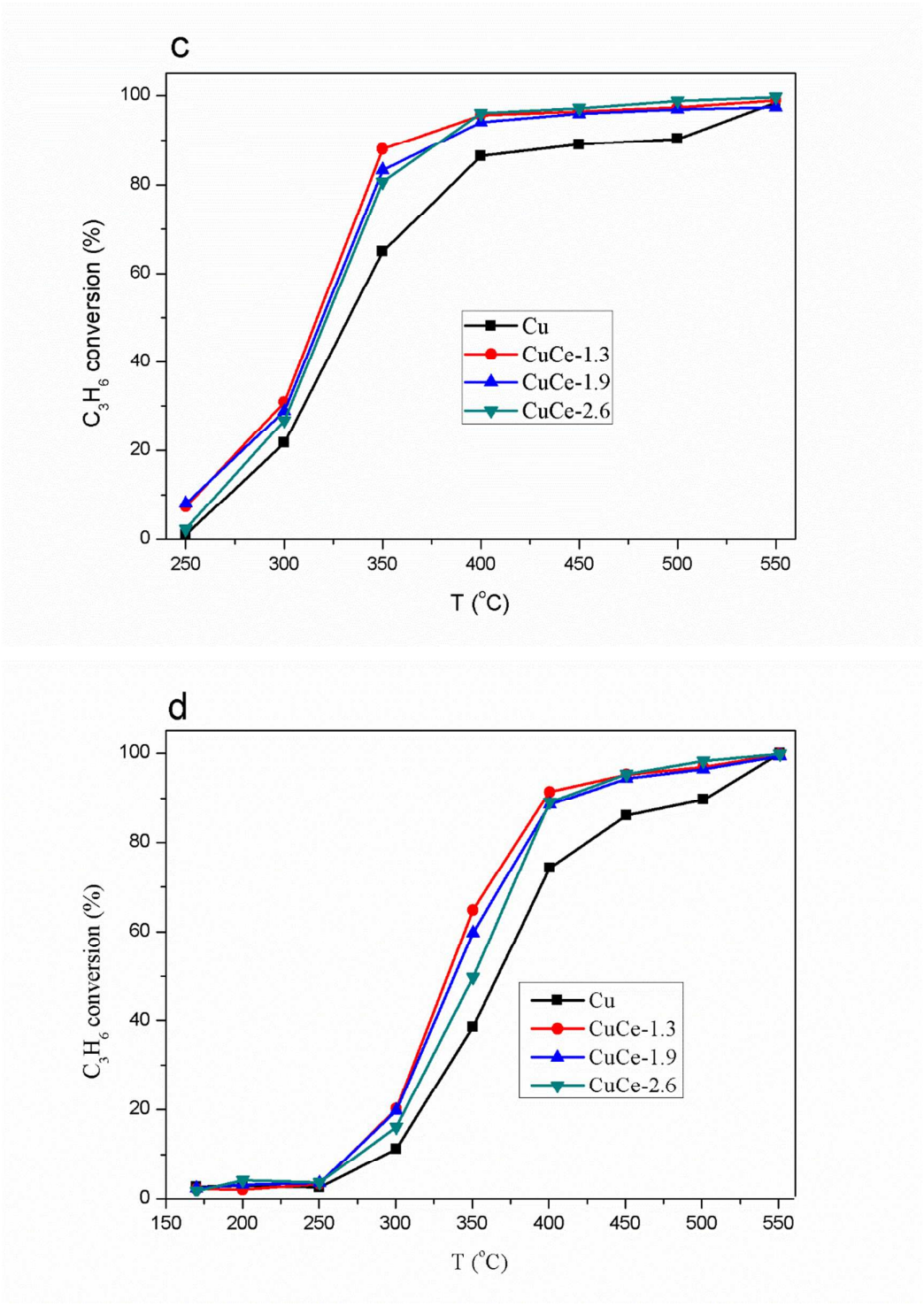

Fig.3

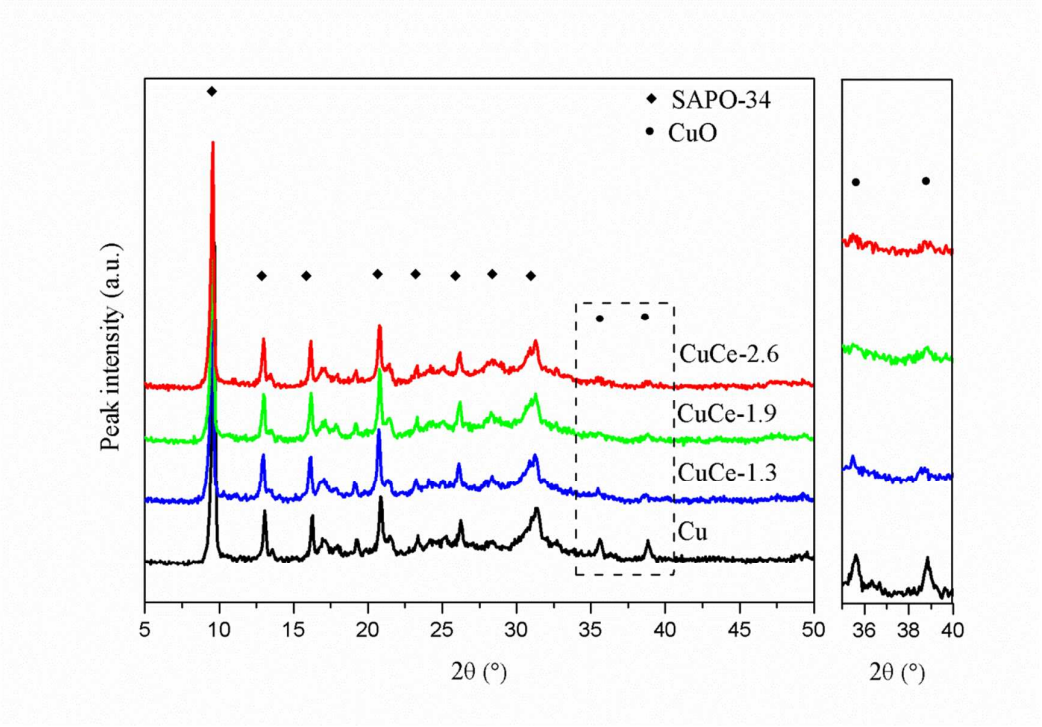

Fig.4

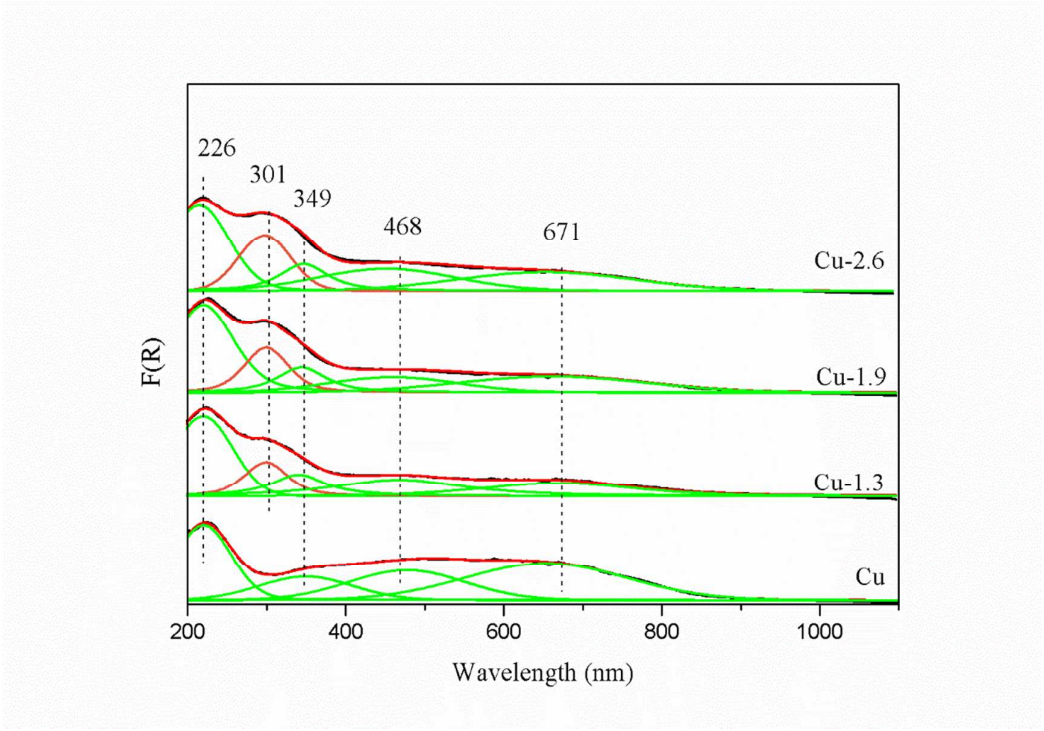

Fig. 5

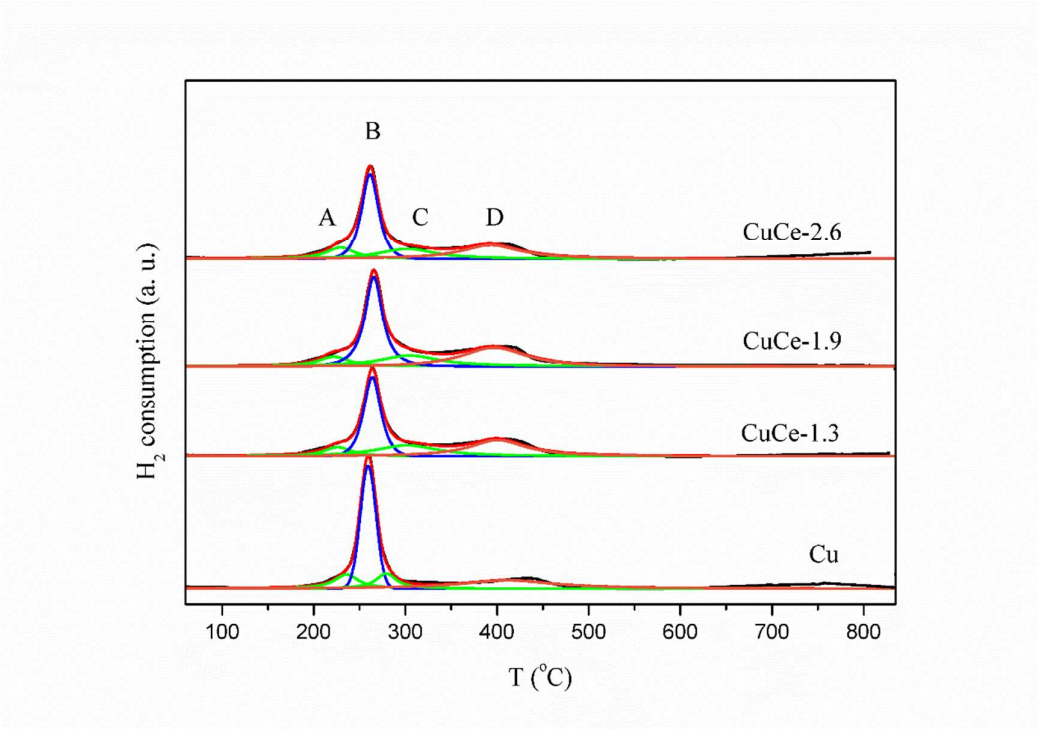

Fig. 6

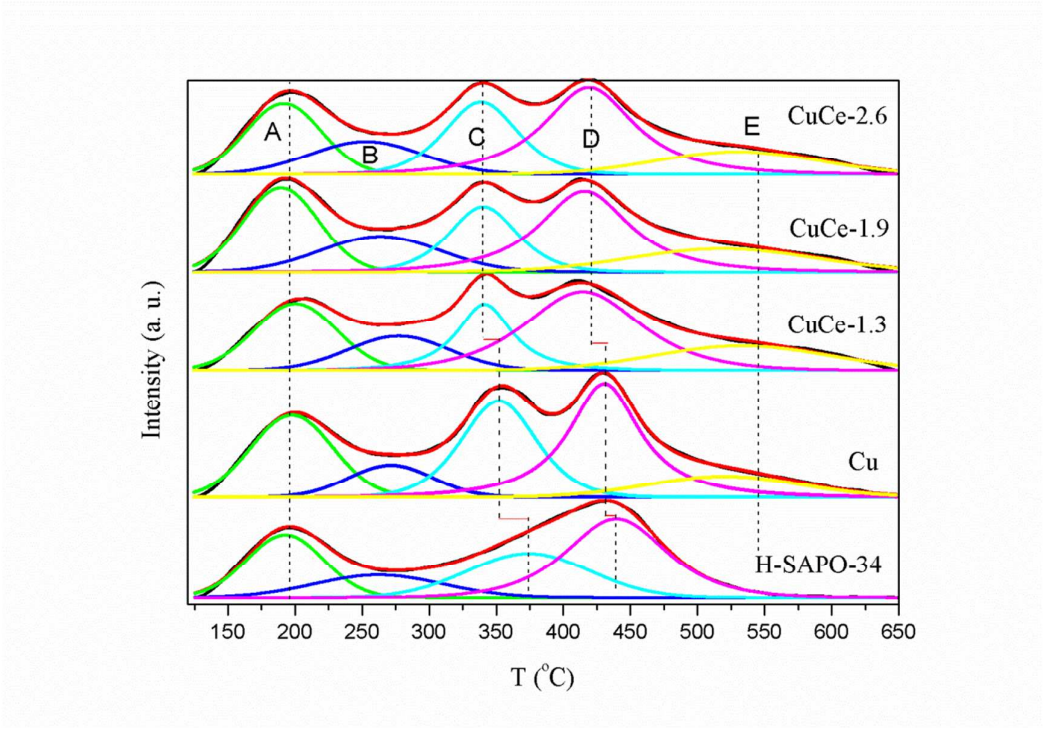

Fig. 7

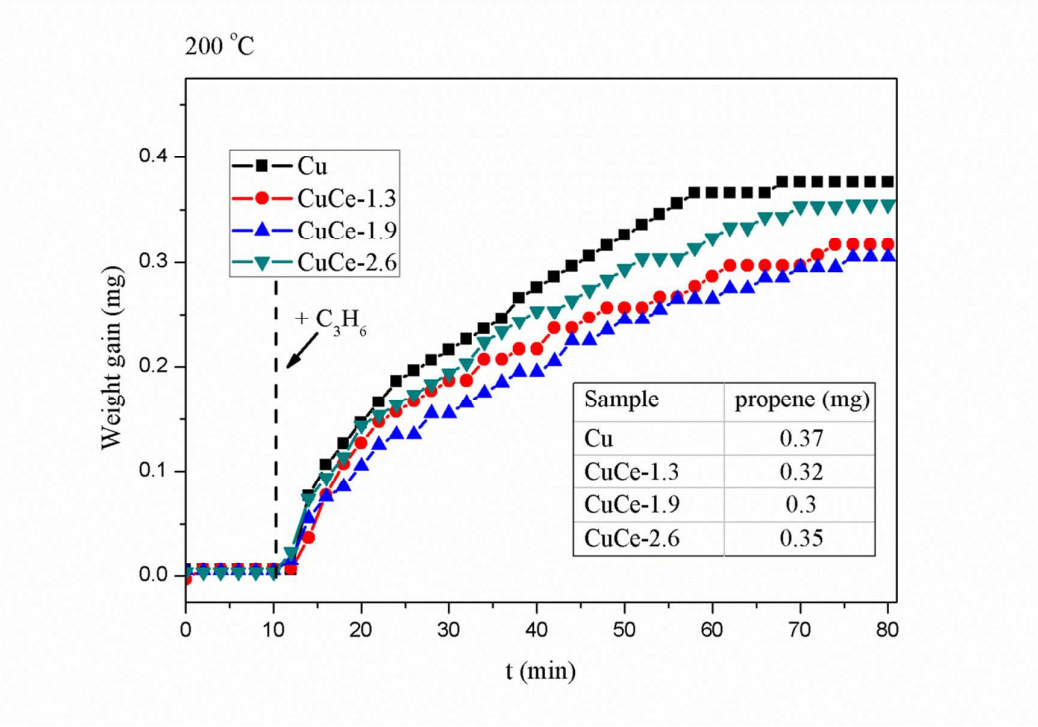

Sample	propene (mg)
Cu	0.37
CuCe-1.3	0.32
CuCe-1.9	0.3
CuCe-2.6	0.35

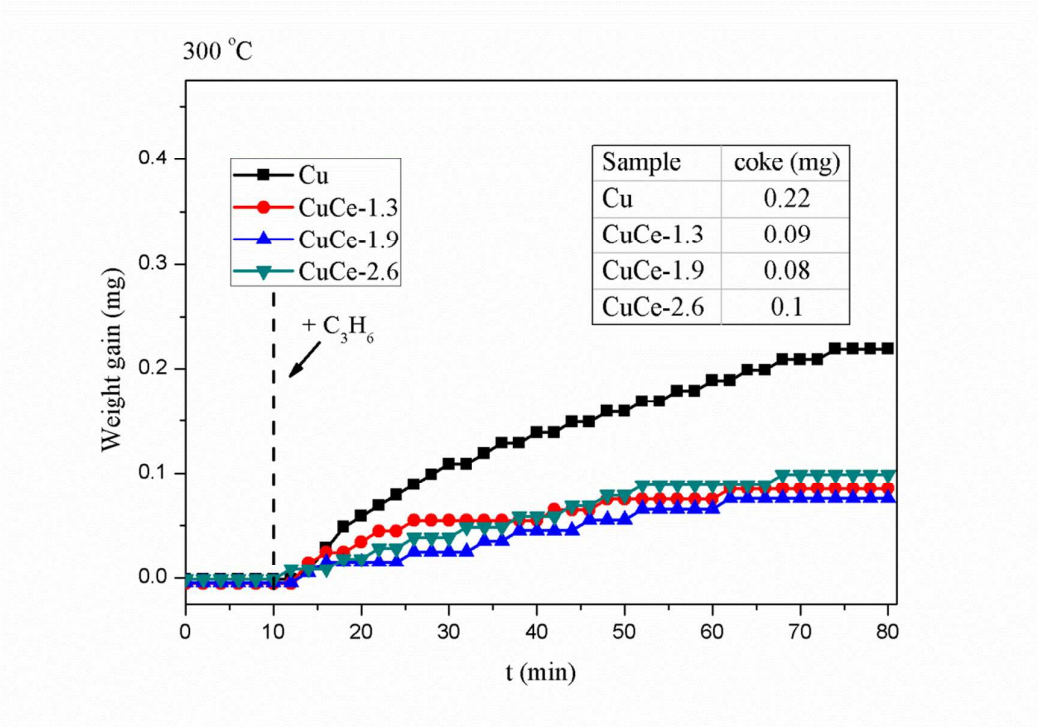

Sample	coke (mg)
Cu	0.22
CuCe-1.3	0.09
CuCe-1.9	0.08
CuCe-2.6	0.1

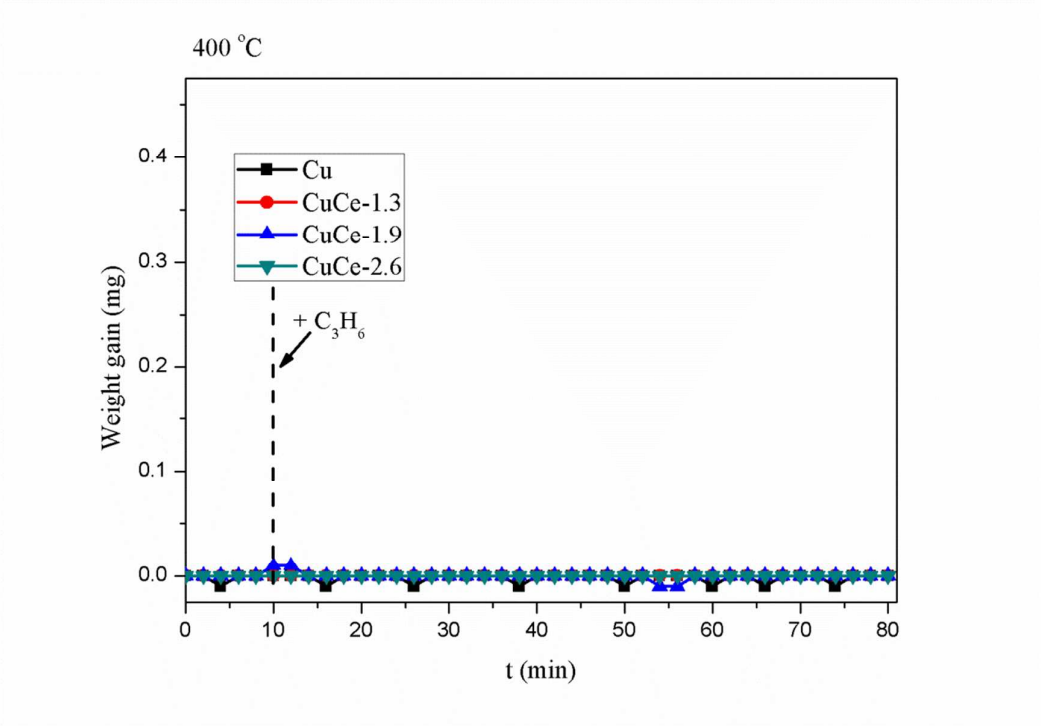

Fig. 8